

NANO EXPRESS

Open Access



# Near-infrared emitting AgInTe<sub>2</sub> and Zn-Ag-In-Te colloidal nanocrystals

Marc-Antoine Langevin<sup>1,2</sup>, Thomas Pons<sup>3</sup>, Anna M. Ritcey<sup>1,2</sup> and Claudine Ni. Allen<sup>2\*</sup>

## Abstract

The synthesis of AgInTe<sub>2</sub> nanocrystals emitting between 1095 nm and 1160 nm is presented. Evolution of the Ag:In:Te ratio shows progressive incorporation of In<sup>3+</sup> in Ag<sub>2</sub>Te, leading to the formation of orthorhombic AgInTe<sub>2</sub>. When zinc is added to the synthesis, the photoluminescence quantum yield reaches 3.4 %.

**Keywords:** Silver indium telluride; I-III-VI semiconductors; Colloidal quantum dots; Near-infrared photoluminescence; Nanocrystal synthesis; Tuneable emission; Ion exchange reaction

## Background

In past years, inorganic semiconductor nanocrystals (NCs), including colloidal quantum dots (cQDs), have gained much interest for their use in many applications such as biological imaging, solar cells, analytical chemistry, etc. [1–3]. Although NCs possess interesting properties such as a broad absorption bandwidth and tuneable emission wavelengths, most of them are based on toxic elements such as cadmium, lead, mercury or arsenic, and are hence limited in their industrial use [4–7]. More recently, NCs based on less toxic elements have also been developed [7–12]. I(Ag,Cu)-III(In,Ga)-VI(S,Se,Te)<sub>2</sub> compounds have been widely studied as bulk materials, principally for their successful use in photovoltaic devices [13]. This has motivated research on nanocrystalline versions in order to generate tuneable electronic and optical properties, especially in the biologically and technologically important near-infrared range of the spectrum [4, 8–10].

In order to harness the full tuning potential of these versatile alloyed nanomaterials, it is necessary to develop new systems and synthetic methods to understand their reactivities. However, with the exception of AgInS<sub>2</sub>, silver-based I-III-VI<sub>2</sub> NCs have mostly been overlooked. We recently presented a method for the synthesis of near-stoichiometric AgInSe<sub>2</sub> NCs via thermolysis of an Ag-In-thiolate complex followed by

an anion-exchange reaction and indium incorporation [12]. This reaction is possible because the P-Se bonds (315 kJ/mol) of the tributylphosphine selenide (TBP-Se) precursor are weaker than the P-S bonds (403 kJ/mol) [14]. In the present communication, we demonstrate the versatility of this route with the first synthesis of AgInTe<sub>2</sub> (AIT) NCs. Since the P-Te bonds (218 kJ/mol) are also weaker than the P-S bonds, the anion-exchange route can be employed for the substitution of Te into the NCs [14].

## Methods

In a typical experiment, 0.025 mmol (5.8 mg) of Ag<sub>2</sub>O and 0.05 mmol (14.6 mg) of In(OAc)<sub>3</sub> were dissolved in 0.25 mL of dodecanethiol (DDT) and 5 mL of octadecene (ODE). After degassing under vacuum at 90 °C for 30 min, 0.25 mL of oleylamine (OLA) was injected in the reaction flask. The solution was then degassed for an additional 30 min and put under N<sub>2</sub> atmosphere using a standard Schlenk-line technique. The solution was heated to an adequate temperature of 170 °C or 200 °C and 0.2 mL of the Te precursor was injected. This Te precursor was prepared by dissolving 0.55 mmol (70 mg) of Te in 0.25 mL of trioctylphosphine (TOP) and 0.75 mL of ODE. The solution turned dark brown immediately after precursor injection. Injecting TBP instead of TOP in the precursor solution caused instant formation of a black precipitate. The suspensions were allowed to react at constant temperature for 180 min. Aliquots were removed at different reaction times and dispersed in tetrachloroethylene (TCE) for absorption,

\* Correspondence: claudine.allen@phy.ulaval.ca

<sup>2</sup>Centre d'Optique, Photonique et Laser (COPL), Département de Physique, de Génie Physique et d'Optique, Université Laval, 2375 Rue de la Terrasse, Quebec, QC G1V 0A6, Canada

Full list of author information is available at the end of the article

photoluminescence (PL) and energy dispersive x-ray (EDS) spectroscopic measurements. The NCs were purified by centrifugation in methanol and dispersed in TCE to obtain stable colloidal suspensions. Other solvents such as ethanol, isopropanol and acetone were tested for centrifugation, but they severely quenched the PL emission intensity.

## Results and discussion

The transmission electron microscopy (TEM) image presented in Fig. 1a shows the presence of 10.6 ( $\sigma = \pm 3$ ) nm AIT NCs. Their shape is approximately spherical with a clear trend to form elongated NCs. As shown in Fig. 1b, X-ray diffraction (XRD) analysis confirms that the AIT NCs are mostly in the metastable orthorhombic phase and free of other inorganic compounds after purification. Since no XRD reference pattern is available for orthorhombic AIT, we compare our diffractogram to orthorhombic  $\text{AgInS}_2$ , which is shifted towards larger angles due to the smaller size of the sulphur anion [15, 16]. The presence of tetragonal phase cannot be completely excluded because all its main diffraction peaks ( $24.0^\circ$ ,  $39.8^\circ$  and  $46.6^\circ$ ) are also found in the orthorhombic phases.

EDS analysis performed on aliquots taken at different reaction times after TOP-Te injection shows progressive

incorporation of  $\text{In}^{3+}$  in  $\text{Ag}_2\text{Te}$  NCs as presented in Table 1 and Fig. 2. This is the same reaction mechanism as that proposed for  $\text{AgInS}_2$  and  $\text{AgInSe}_2$  NCs in the orthorhombic phase [12, 17]. Similar incorporation mechanisms were also recently observed for  $\text{CuInS}_2$  NCs [18, 19]. The final AIT NCs are near-stoichiometric and contain, at most,  $6.4 \pm 0.3$  % of sulphur, which can be attributed to the remaining DDT present as a surface ligand. Here,  $\text{Ag}_2\text{Te}$  NCs are likely to result from an anion-exchange reaction on  $\text{Ag}_2\text{S}$  formed after thermolysis of the Ag-In-thiolate complex. Even though it was not possible to isolate  $\text{Ag}_2\text{S}$  NCs at this step of the reaction, an equivalent anion-exchange reaction was attempted on pure  $\sim 4$  nm  $\text{Ag}_2\text{S}$  NCs [20] dispersed in ODE with OLA and DDT to demonstrate that this exchange is indeed possible.  $\text{Ag}_2\text{Te}$  was instantly obtained when TOP-Te was injected at  $170^\circ\text{C}$  as demonstrated by XRD (Additional file 1: Figure S1 of the supporting information).

As presented in Fig. 3a, b, this method allows tuning of the AIT NCs' emission wavelength between 1160 nm and 1095 nm, depending on the reaction temperature and time. At  $170^\circ\text{C}$ , a rapid redshift of the PL peak is observed during the first three minutes of reaction. This is immediately followed by a blueshift, which slows down progressively, reaching a plateau at 1100 nm after 60 min of reaction. The suspension was allowed to react for six more hours, but no significant changes were observed in either the PL spectrum or the composition as monitored by EDS. At  $200^\circ\text{C}$ , we did not observe the initial redshift, possibly because of the faster reaction kinetics.

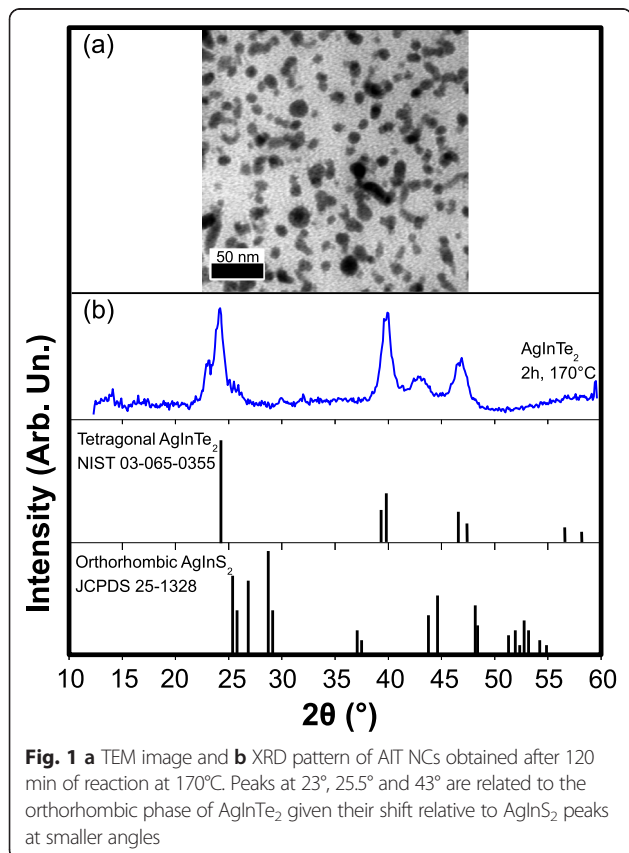
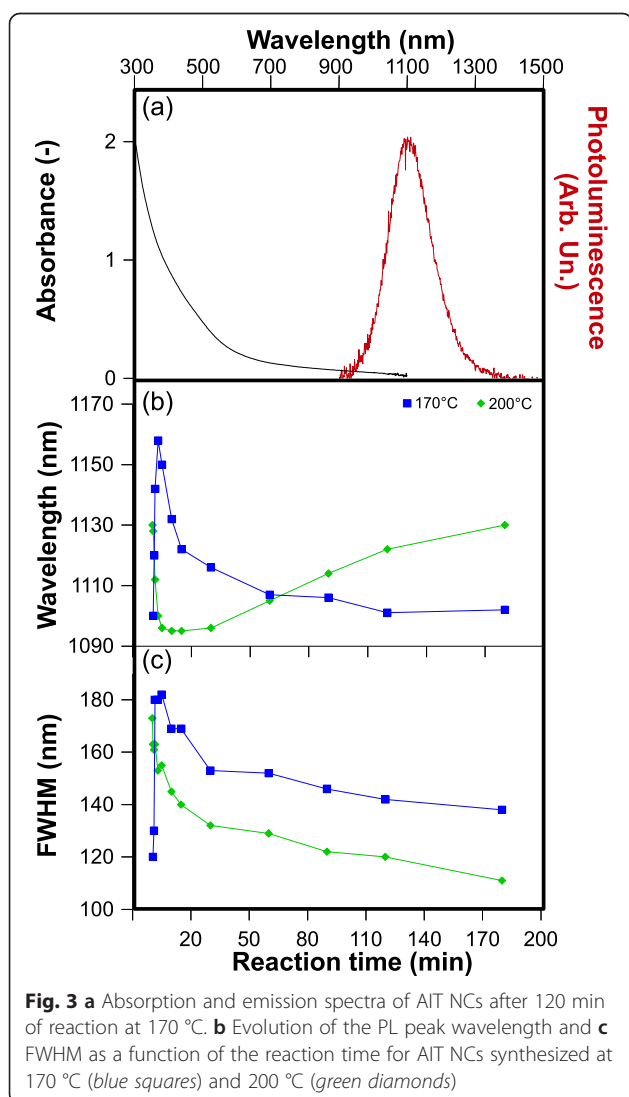
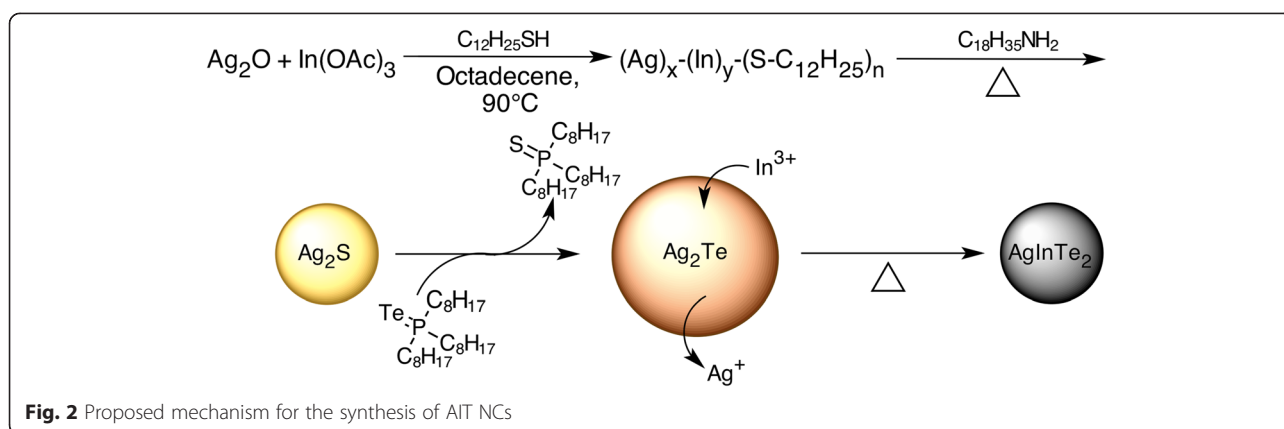


**Fig. 1** a TEM image and b XRD pattern of AIT NCs obtained after 120 min of reaction at  $170^\circ\text{C}$ . Peaks at  $23^\circ$ ,  $25.5^\circ$  and  $43^\circ$  are related to the orthorhombic phase of  $\text{AgInTe}_2$  given their shift relative to  $\text{AgInS}_2$  peaks at smaller angles

**Table 1** Percentage of Ag, In, Te and S in AIT NCs synthesized at  $170^\circ\text{C}$  and  $200^\circ\text{C}$  measured by energy dispersive x-ray spectroscopy

Reaction temperature	Reaction time (min)	% Ag	% In	% Te	% S
$170^\circ\text{C}$	0.5	$57 \pm 1$	$8 \pm 1$	$30 \pm 1$	$5.5 \pm 0.6$
	1	$44 \pm 2$	$18 \pm 2$	$35 \pm 2$	$2.9 \pm 0.2$
	5	$38 \pm 3$	$18.1 \pm 0.1$	$40 \pm 2$	$4.5 \pm 0.9$
	15	$28.9 \pm 0.3$	$24 \pm 2$	$42 \pm 2$	$5.0 \pm 0.5$
	30	$26.8 \pm 0.7$	$23.4 \pm 0.9$	$44.1 \pm 0.3$	$5.6 \pm 0.2$
	60	$24.7 \pm 0.3$	$25.2 \pm 0.6$	$44.4 \pm 0.6$	$5.8 \pm 0.1$
	120	$24 \pm 1$	$27 \pm 1$	$43.6 \pm 0.4$	$6.4 \pm 0.3$
$200^\circ\text{C}$	0.5	$44 \pm 3$	$20 \pm 2$	$32 \pm 1$	$2.2 \pm 0.6$
	1	$44 \pm 2$	$17 \pm 2$	$34 \pm 7$	$2.6 \pm 0.5$
	5	$34 \pm 4$	$24 \pm 3$	$38 \pm 8$	$3 \pm 1$
	10	$29.0 \pm 0.9$	$34 \pm 2$	$33.4 \pm 0.9$	$3.3 \pm 0.8$
	15	$24 \pm 3$	$36 \pm 3$	$37 \pm 1$	$3.1 \pm 0.1$
	30	$22 \pm 1$	$35 \pm 2$	$39 \pm 2$	$3 \pm 1$
	120	$24.8 \pm 0.4$	$34.3 \pm 0.4$	$37 \pm 1$	$4 \pm 1$



We only observed a rapid blueshift, from 1130 nm to 1095 nm after 5 min, followed by a progressive redshift beginning after 30 min of reaction. NC size distributions are obtained from TEM analysis (Additional file 1: Figure S2) of aliquots prepared under the reaction conditions indicated in Table 2. Their ensemble average and its uncertainty were evaluated by bootstrapping sampling and the results indicate a correlation between NC size and PL emission wavelength, which is graphically confirmed by Additional file 1: Figure S3 in the supporting information. At both reaction temperatures, longer reaction times are also associated to a narrower FWHM of the PL emission spectra (Fig. 3c) and improved relative size dispersion ( $\sigma$ ) of NCs (Table 2). To avoid errors that could be induced by NC ripening or other changes during storage, PL measurements and TEM grid preparations were carried out immediately after the synthesis.

To explain these results, we consider the PL emission mechanisms of I-III-VI<sub>2</sub> NCs which are complex due to the involvement of defect states and thus depend on the exact stoichiometry for a given crystal structure [21]. These mechanisms fall in two categories: donor-acceptor pair recombination or a transition between one of these defect states and one of the semiconductor bands. If the latter type of mechanisms prevails, it could provide an

**Table 2** Evolution of the NC size distributions, determined by TEM, and corresponding PL emission wavelengths

Temperature (°C)	Time (min)	NC size (nm)	$\sigma$ (nm)	Wavelength (nm)
	0.5	10.6±0.4	3	1100
170	3	15±1	6	1158
	120	10.7±0.4	3	1101
	0.2	13±1	4	1130
200	30	10.3±0.5	2	1096
	230	12.8±0.5	2	1122

explanation for the observed spectral shifts and line-width changes. Finally, we briefly compare the emission characteristics of AgInTe<sub>2</sub> NCs with those previously reported for AgInSe<sub>2</sub>. In the bulk, the bandgap of the two materials differs by ~0.3 eV [22]. Both nanomaterials emit in the same range of wavelengths for NCs with a similar ~10 nm size. However, the FWHM is much narrower for NCs with Te (124 nm) instead of Se (357 nm) anions, despite the similar size polydispersity (~25 %) of the two populations [12].

The PL quantum yield (QY) was evaluated relative to ICG (13 % in DMSO) [8]. A maximum PL QY of 0.06 % was measured for AIT NCs synthesized at 170 °C after 120 min reaction. The PL, however, was completely quenched after a single day of storage in ambient conditions, most likely because of surface oxidation often observed for Te-based NCs [23]. Indeed, when kept under a N<sub>2</sub> atmosphere, the NCs still emitted light after 2 months. Previous studies have shown that it is possible to increase the PL QY of I-III-VI<sub>2</sub> NCs by incorporating zinc [24]. Therefore, starting from our protocol for AIT NCs synthesized at 170 °C, we added either 0.025 mmol (5.5 mg) or 0.05 mmol (11.0 mg) of Zn(OAc)<sub>2</sub>·2H<sub>2</sub>O in the initial mixture in order to study the characteristics of Zn-Ag-In-Te solid solution NCs. This corresponds to Zn:Ag ratios of 0.5:1 and 1:1, respectively, and after 120 min of reaction, both samples contained NCs with similar sizes. Indeed, the size distributions measured from the TEM images in Fig. 4a and b are 9 (σ = ±2) nm and 11 (σ = ±2) nm for Zn:Ag ratios of 0.5:1 and 1:1 respectively. We recorded PL spectra centered between 1045 nm and 1095 nm in the former case and between 940 nm and 1005 nm in the latter case, as presented in Fig. 4c. The complete series of PL spectra as a function of reaction time is provided in the supporting information (Additional file 1: Figure S4). The XRD diffractograms recorded for both samples were almost identical to those of AIT NCs (Additional file 1: Figure S5), without any signature of other inorganic compounds after purification. The PL QY relative to ICG was evaluated for both samples. The expected increase in radiative emission for these Zn-Ag-In-Te NCs was observed with a PL QY of 2.7 % for a Zn:Ag ratio of 0.5:1 and of 3.4 % for a Zn:Ag ratio of 1:1 after 180 min of reaction. However, the PL was still quickly quenched when the NCs were exposed to air.

## Conclusions

In summary, we prepared for the first time near-stoichiometric AgInTe<sub>2</sub> NCs emitting in the NIR via a versatile route involving thermolysis of an Ag-In-thiolate complex and progressive incorporation of In<sup>3+</sup>. When Zn(OAc)<sub>2</sub> was added at the beginning of the synthesis, a significant increase in PL QY up to 3.4 % was observed for a Zn:Ag ratio

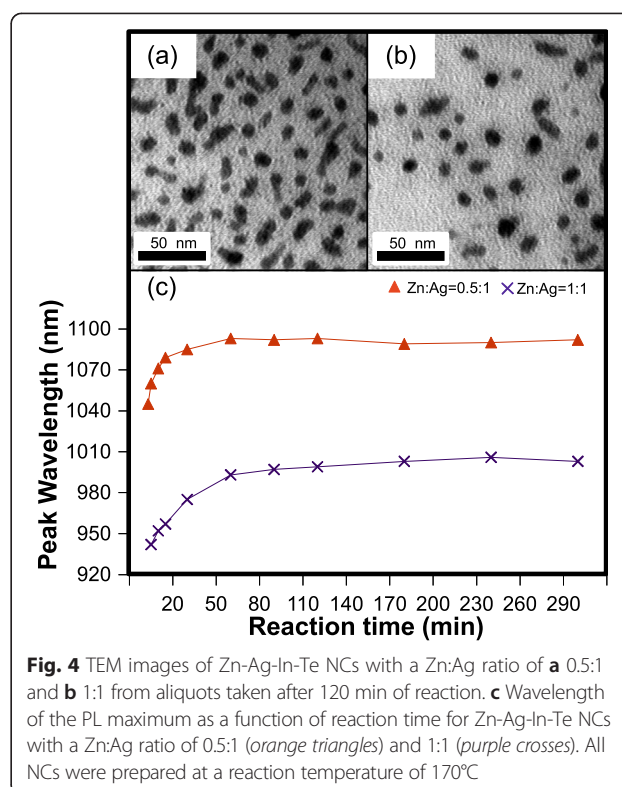


**Fig. 4** TEM images of Zn-Ag-In-Te NCs with a Zn:Ag ratio of **a** 0.5:1 and **b** 1:1 from aliquots taken after 120 min of reaction. **c** Wavelength of the PL maximum as a function of reaction time for Zn-Ag-In-Te NCs with a Zn:Ag ratio of 0.5:1 (orange triangles) and 1:1 (purple crosses). All NCs were prepared at a reaction temperature of 170 °C

of 1:1. In all instances, the NCs were quickly oxidized inducing PL quenching after 1 day of storage. Therefore, further work will be needed in order to increase air stability of AgInTe<sub>2</sub> and Zn-Ag-In-Te NCs.

## Additional file

**Additional file 1: Supporting information.** The file contains Chemicals, Equipment, Analysis methods and Figures S1 to S5.

### Abbreviations

NCs: Nanocrystals; cQDs: Colloidal quantum dots; TBP: Tributylphosphine; AIT: AgInTe<sub>2</sub>; DDT: Dodecanethiol; ODE: Octadecene; OLA: Oleylamine; TOP: Trioctylphosphine; TCE: Tetrachloroethylene; PL: Photoluminescence; EDS: Energy-dispersive X-ray spectroscopy; TEM: Transmission electron microscopy; XRD: X-ray diffraction; QY: Quantum yield; ICG: Indocyanine green.

### Competing interests

The authors declare that they have no competing interests.

### Authors' contributions

TP, AMR and CNA proposed ideas and presided over the study. MAL conceived and designed the experiments and drafted the manuscript. All authors read and approved the final manuscript.

### Acknowledgements

The authors thank Samuel Tremblay, Patrick Larochelle, Stéphan Gagnon, Rodica N. Plesu, and Wenhua Bi for technical support. This work was supported by the Fonds de Recherche du Québec-Nature et Technologies (FRQ-NT).

### Author details

<sup>1</sup>Centre de Recherche sur les Matériaux Avancés (CERMA), Département de Chimie, Université Laval, 1045 Av. de la Médecine, Québec, QC G1V 0A6,

Canada. <sup>2</sup>Centre d'Optique, Photonique et Laser (COPL), Département de Physique, de Génie Physique et d'Optique, Université Laval, 2375 Rue de la Terrasse, Québec, QC G1V 0A6, Canada. <sup>3</sup>Laboratoire Physique et Étude des Matériaux, ESPCI/CNRS/UPMC UMR8213, 10 Rue Vauquelin, 75005 Paris, France.

Received: 7 April 2015 Accepted: 21 May 2015

Published online: 05 June 2015

## References

1. Michalet X, Pinaud FF, Bentolila L, Tsay JM, Doose S, Li JJ, et al. Quantum dots for live cells, in vivo imaging, and diagnostics. *Science*. 2005;307:538–44.
2. Li W, Pan Z, Zhong X. CuInSe<sub>2</sub> and CuInSe<sub>2</sub>-ZnS based high efficiency "green" quantum dot sensitized solar cells. *J Mater Chem A*. 2015;3:1649–55.
3. Lecavalier MÈ, Goulet M, Allen CN, Beaulieu L, Larivière D. Water-dispersible colloidal quantum dots for the detection of ionizing radiation. *Chem Commun*. 2013;49:11629–31.
4. Kim S, Lim YT, Soltesz EG, De Grand AM, Lee J, Nakayama A, et al. Near-infrared fluorescent type II quantum dots for sentinel lymph node mapping. *Nat Biotechnol*. 2004;22:93–7.
5. Harris DK, Allen PM, Han HS, Walker BJ, Lee J, Bawendi MG. Synthesis of cadmium arsenide quantum dots luminescent in the infrared. *J Am Chem Soc*. 2011;133:4676–9.
6. Keuleyan S, Lhuillier E, Guyot-Sionnest P. Synthesis of colloidal HgTe quantum dots for narrow mid-IR emission and detection. *J Am Chem Soc*. 2011;133:16422–4.
7. van Veggel FCJM. Near-infrared quantum dots and their delicate synthesis, challenging characterization, and exciting potential applications. *Chem Mater*. 2014;26:111–22.
8. Pons T, Pic E, Lequeux N, Cassette E, Bezdetnaya L, Guillemin F, et al. Cadmium-free CuInS<sub>2</sub>/ZnS quantum dots for sentinel lymph node imaging with reduced toxicity. *ACS Nano*. 2010;4:2531–8.
9. Zhong H, Wang Z, Bovero E, Lu Z, van Veggel FCJM, Scholes GD. Colloidal CuInSe<sub>2</sub> nanocrystals in the quantum confinement regime: synthesis, optical properties, and electroluminescence. *J Phys Chem C*. 2011;115:12396–402.
10. Kim S, Kang M, Kim S, Heo JH, Noh JH, Im SH, et al. Fabrication of CuInTe<sub>2</sub> and CuInTe<sub>(2-x)</sub>Se<sub>(x)</sub> ternary gradient quantum dots and their application to solar cells. *ACS Nano*. 2013;7:4756–63.
11. Hamanaka Y, Ogawa T, Tsuzuki M. Photoluminescence properties and its origin of AgInS<sub>2</sub> quantum dots with chalcopyrite structure. *J Phys Chem C*. 2011;115:1786–92.
12. Langevin MA, Ritcey AM, Allen CN. Air-stable near-infrared AgInSe<sub>2</sub> nanocrystals. *ACS Nano*. 2014;8:3476–82.
13. Banger KK, Jin MHC, Harris JD, Fanwick PE, Hepp AF. A new facile route for the preparation of single-source precursors for bulk, thin-film, and nanocrystallite I–III–VI semiconductors. *Inorg Chem*. 2003;42:7713–5.
14. Saruyama M, Yeong-Gi S, Kimoto K, Taguchi S, Kanemitsu Y, Teranishi T. Spontaneous formation of wurzite-CdS/zinc blende-CdTe heterodimers through a partial anion exchange reaction. *J Am Chem Soc*. 2011;133:17598–601.
15. Kasiviswanathan S, Krishna Rao D, Gopalam BSV. Preparation and characterization of the pseudobinary system Cu<sub>1-x</sub>Ag<sub>x</sub>InTe<sub>2</sub>. *J Mater Sci Lett*. 1986;5:912–9. NIST 03-065-0355.
16. Swarthmore P. Powder diffraction file alphabetical index. Inorganic phases. Newtown Square, PA: JCPDS-International Centre for Diffraction Data; 1980.
17. Ogawa T, Kuzuya T, Hamanaka Y, Sumiyama K. Synthesis of Ag-In binary sulfide nanoparticles-structural tuning and their photoluminescence properties. *J Mater Chem*. 2010;20:2226–31.
18. van der Stam W, Berends AC, Rabouw FT, Wilhammar T, Ke X, Meeldijk JD, et al. Luminescent CuInS<sub>2</sub> Quantum Dots by Partial Cation Exchange in Cu<sub>2</sub>-xS Nanocrystals. *Chem Mater*. 2015;27:621–8.
19. Leach ADP, Mast LG, Hernández-Pagán EA, Macdonald JE. Phase dependent visible to near-infrared photoluminescence of CuInS<sub>2</sub> nanocrystals. *J Mater Chem C*. 2015;3:3258–65.
20. Zhang Y, Liu Y, Li C, Chen X, Wang Q. Controlled Synthesis of Ag<sub>2</sub>S Quantum Dots and Experimental Determination of the Exciton Bohr Radius. *J Phys Chem C*. 2014;118:4918–23.
21. Aldakov D, Lefrançois A, Reiss P. Ternary and quaternary metal chalcogenide nanocrystals: synthesis, properties and applications. *J Mater Chem C*. 2013;1:3756–76.
22. Bellabarba C, Gázquez J, Ricón C, Quintero M. Photoconductivity and valence band structure of AgInTe<sub>2</sub>. *Solid State Commun*. 1986;58:243–6.
23. Wuister SF, van Driel F, Meijerink A. Luminescence and growth of CdTe quantum dots and clusters. *Phys Chem Chem Phys*. 2003;5:1253–8.
24. Chang JY, Wang GQ, Cheng CY, Lin WX, Hsu JC. Strategies for photoluminescence enhancement of AgInS<sub>2</sub> quantum dots and their application as bioimaging probes. *J Mater Chem*. 2012;22:10609–18.

**Submit your manuscript to a SpringerOpen<sup>®</sup> journal and benefit from:**

- Convenient online submission
- Rigorous peer review
- Immediate publication on acceptance
- Open access: articles freely available online
- High visibility within the field
- Retaining the copyright to your article

Submit your next manuscript at ► [springeropen.com](http://springeropen.com)